LINEAR AND NONLINEAR EFFECTS OF FRINGE FIELDS ON THE SINGLE-PARTICLE DYNAMICS IN THE HELIUM LIGHT ION COMPACT SYNCHROTRON

S. Van der Schueren*, R. De Maria, H. Huttunen, European Organization for Nuclear Research, Geneva, Switzerland
M. Migliorati, Istituto Nazionale di Fisica Nucleare, Rome, Italy
V. Korchevnyuk, École Polytechnique Fédérale de Lausanne, Lausanne, Switzerland

Abstract

The Helium Light-Ion Compact Synchrotron (HeLICS) is a proposed cancer treatment facility developed within the Next Ion Medical Machine Study (NIMMS) at CERN, designed both for clinical treatment with protons and research with helium ions. Consisting of a triangular lattice with six 60° combined-function magnets with 30° edge angles, this machine challenges the current treatment of fringe fields in beam dynamics simulations. At present, accurate maps for the fringe fields of curved combined-function magnets with edge angles are not available in the literature. In this work we investigate the linear and non-linear effects of these fringe fields through the framework of resonance driving terms, providing an alternative approach to quantify their influence on single-particle dynamics.

INTRODUCTION

The current design of the HeLICS ring [1] is a triangular lattice with a circumference of 35 m, designed to accelerate alpha particles from 5 MeV/u to 220 MeV/u [2, 3]. In machines of this scale, fringe fields can have a significant impact on the beam optics, while the effects are often only taken into account in a late stage of the design of the machine when a magnetic field map is available. Our goal is to develop methods to study the impact of existing combined-function magnets, but also produce field-quality specifications for magnets to be designed, therefore accounting for fringe field effects earlier in the ring design process.

THE HELICS SYNCHROTRON

The HeLICS optics [4], computed with Xsuite [5] and shown in Fig. 1, contains six combined-function dipole-quadrupole magnets with design parameters given in Tab. 1. Since the machine is still in the design phase, a final design and three-dimensional field map of the dipoles are not available.

Field map of the HeLICS dipole

Since an up-to-date HeLICS magnet design is still ongoing, we decided to introduce a generated field map based on a general magnetic field expansion in Frenet-Serret coordinates [6],

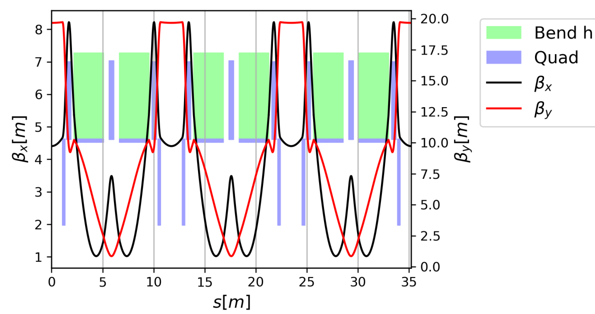

Figure 1: HeLICS optics with $Q_x = 2.39, Q_y = 1.21$.

Table 1: Design Parameters for the Combined-Function Dipoles in the Current Design of the HeLICS Ring

Parameter	**Design value**
bending radius	2.74 m
bending angle	60 degrees
edge angle	30 degrees
(curved) magnetic length	2.87 m
dipole strength	1.65 T
quadrupole strength	-0.50 T/m

$$\vec{R}(x, y, s) = \vec{R}_0(s) + x\hat{x}(s) + y\hat{y}(s) \tag{1}$$

$$\frac{d}{ds}\vec{R}_0(s) = \hat{s}(s)\ , \tag{2}$$

with $\vec{R}$ the position of the particle, $\vec{R}_0$ the reference trajectory, and $\hat{x}$ and $\hat{y}$ the horizontal and vertical unit vectors of a coordinate system anchored to the reference trajectory. We have that $\hat{s} = \vec{R}_0'(s), \hat{x}'(s) = h(s)\hat{s}(s)$ and $\hat{y}(s) = -\hat{x}(s)\times\hat{s}(s)$ and $h(s) = 1/\rho(s)$ is the local curvature, see Fig. 2.

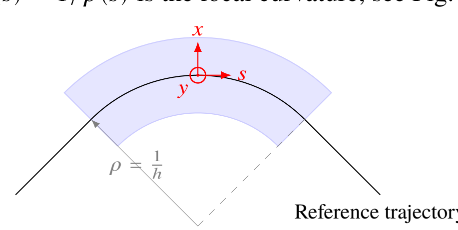

Figure 2: The Frenet-Serret reference frame to describe the combined-function dipole is straight outside of the magnetic length, and bent with bending radius $\rho = \frac{1}{h}$ inside the magnetic length.

The magnetic field will be specified in terms of derivatives on axis (Taylor coefficients),

* silke.van.der.schueren@cern.ch

$$a_n(s) = \partial_x^{n-1} B_x(x,y,s)\big|_{x=y=0} \tag{3}$$
$$b_n(s) = \partial_x^{n-1} B_y(x,y,s)\big|_{x=y=0} \tag{4}$$
$$b_s(s) = B_s(x=0, y=0, s) \tag{5}$$

from which the total magnetic field can be reconstructed from the scalar potential $\mathbf{B} = -\nabla\Phi$ [7]

$$\Phi(x,y,s) = \sum_{i=0}^{\infty} \phi_i(x,s)\frac{y^i}{i!}, \tag{6}$$

where ϕ_i are functions satisfying the recursion relation

$$\phi_{i+2} = -\frac{1}{1+hx}\left(\partial_x\left((1+hx)\partial_x\phi_i\right) + \partial_s\left(\frac{1}{1+hx}\partial_s\phi_i\right)\right) \tag{7}$$

with initial functions ϕ_0 and ϕ_1,

$$\phi_0(x,s) = -a_0(s) - \sum_{n=1}^{\infty} a_n(s)\frac{x^n}{n!} \tag{8}$$
$$\phi_1(x,s) = -\sum_{n=1}^{\infty} b_n(s)\frac{x^{n-1}}{(n-1)!}. \tag{9}$$

For our combined-function magnet, we chose a constant b_1 and b_2 in curvilinear frame according to the design parameters, from which a field map at the midplane was created. The 30° edge angle was included by multiplying this field map with an Enge function [9] for which the ELENA dipole [10, 11] (fitted and rescaled with the magnet gap) served as a model, and will introduce higher-order components around the edge. An illustration of $b_1(s), b_2(s), b_3(s)$ can be found in Fig. 3, the design values in the body will be referred to as $\bar{b}_1, \bar{b}_2, \bar{b}_3$. Note that the components include all the edge effects and no additional steps such as reference frame transformation or hard-soft edge maps are needed.

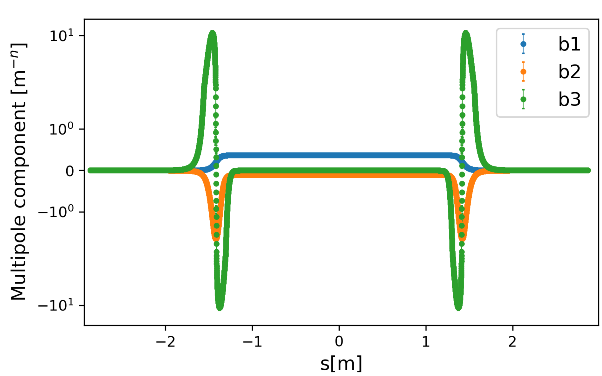

Figure 3: Lowest order multipole components of the created HeLICS dipole field map.

FRINGE FIELD RESONANCE DRIVING TERMS

The non-linear dynamics of a machine can be analysed using the perturbative framework of resonance driving terms [8]. In this framework, one defines the first order resonance driving terms for normal and skew integrated multipole strengths $b_{w,n}$, $a_{w,n}$,

$$f_{jklm}(s) = \frac{\sum_w h_{w,jklm} e^{i[j-k]\Delta\phi^{(s)}_{w,x} + (l-m)\Delta\phi^{(s)}_{w,y}]}}{1 - e^{2\pi i[(j-k)Q_x + (l-m)Q_y]}} \tag{10}$$

with $\Delta\phi^{(s)}_{w,q}$ the phase advance between the source and observation point, and

$$h_{w,jklm} = -\frac{b_{w,n}\Omega(l+m) + i a_{w,n}\Omega(l+m+1)}{j!\,k!\,l!\,m!\,2^{j+k+l+m}} \times i^{l+m}(\beta_{w,x})^{\frac{j+k}{2}}(\beta_{w,y})^{\frac{l+m}{2}} \tag{11}$$

with $\Omega(i) = 1$ if i is even, and 0 if i is odd. The coordinates can then be reconstructed using complex Courant-Snyder coordinates $h_{q,\pm} = \tilde{q} \pm i\tilde{p}_q$ with $\tilde{q}, \tilde{p}$ the normalized coordinates, and

$$\begin{aligned} h_{x,-} = {} & \sqrt{2I_x}e^{i(2\pi Q_x N + \psi_{s,x,0})} \\ & - 2i\sum_{jklm} j f^{(s)}_{jklm}(2I_x)^{\frac{j+k-1}{2}}(2I_y)^{\frac{l+m}{2}} \\ & \times e^{i[(1-j+k)(2\pi Q_x N + \psi_{s,x,0}) + (m-l)(2\pi Q_y N + \psi_{s,y,0})]} \end{aligned} \tag{12}$$

$$\begin{aligned} h_{y,-} = {} & \sqrt{2I_y}e^{i(2\pi Q_y N + \psi_{s,y,0})} \\ & - 2i\sum_{jklm} l f^{(s)}_{jklm}(2I_x)^{\frac{j+k}{2}}(2I_y)^{\frac{l+m-1}{2}} \\ & \times e^{i[(k-j)(2\pi Q_x N + \psi_{s,x,0}) + (1-l+m)(2\pi Q_y N + \psi_{s,y,0})]}. \end{aligned} \tag{13}$$

In the case of a strongly curved combined-function magnets with fringe fields, both the curvature of the reference frame and the longitudinal dependence of the field will introduce additional terms in the Hamiltonian, and hence additional resonance driving terms.

Fringe fields

For an s-dependent field in a reference frame with curvature $h(s) = \bar{b}_1\Theta(s)$, where $\Theta(s)$ is a step function that is zero outside the magnet and one inside the magnet, the transverse Hamiltonian is given by

$$H = -(1+hx)\left(\sqrt{(1+\delta)^2 - (p_x - a_x)^2 - p_y^2} + a_s\right) \tag{14}$$

with vector potential up to third order terms, derived from the scalar potential using the formulas from Eq. 15 in [12],

$$\begin{aligned} a_x &= \frac{y^2}{2(1+hx)}b_1' - \frac{xy^2}{2(1+hx)}b_2' \\ a_s &= -\frac{x + \frac{h}{2}x^2}{1+hx}b_1 + \left(\frac{y^2}{2} - \frac{h\frac{x^3}{3} + \frac{x^2}{2}}{1+hx}\right)b_2 + \frac{xy^2}{2}b_3. \end{aligned} \tag{15}$$

The unperturbed Hamiltonian for this system is given by

$$\begin{aligned} H = {} & \frac{p_x^2 + p_y^2}{2} + \bar{b}_1\Theta(s)\frac{x^2}{2} \\ & + \left(\bar{b}_2\Theta(s) - \bar{b}_1\tan\theta\ \left(\delta(s_1) + \delta(s_2)\right)\right)\frac{(x^2 - y^2)}{2} \end{aligned} \tag{16}$$

Table 2: Hamiltonian Terms from First Order Perturbation Theory Resonance Driving Terms

Hamiltonian term	Value for a Combined-Function Magnet in Piecewise Curved Frame
$h_{1000} = h_{0100}$	$-\frac{\sqrt{\beta_x}}{2}(b_1(s) - \bar{b}_1\Theta(s))$
$h_{1100} = 2h_{2000} = 2h_{0200}$	$-h(s)\frac{\beta_x}{4}(b_1(s) - \bar{b}_1) - \frac{\beta_x}{4}\left(b_2(s) - \left(\bar{b}_2\Theta(s) - \bar{b}_1 \tan\theta \ \ (\delta(s_1) + \delta(s_2))\right)\right)$
$h_{0011} = 2h_{0020} = 2h_{0002}$	$\frac{\beta_y}{4}\left(b_2(s) - \left(\bar{b}_2\Theta(s) - \bar{b}_1 \tan\theta \ \ (\delta(s_1) + \delta(s_2))\right)\right)$
$h_{1011} = 2h_{1020} = 2h_{1002}$	$\frac{1}{8}\frac{\beta_y}{\sqrt{\beta_x}}(\alpha_x + i)b_1'(s) + h(s)\frac{\sqrt{\beta_x}\beta_y}{8}b_2(s) + \frac{\sqrt{\beta_x}\beta_y}{8}b_3(s)$
$h_{0111} = 2h_{0120} = 2h_{0102}$	$\frac{1}{8}\frac{\beta_y}{\sqrt{\beta_x}}(\alpha_x - i)b_1'(s) + h(s)\frac{\sqrt{\beta_x}\beta_y}{8}b_2(s) + \frac{\sqrt{\beta_x}\beta_y}{8}b_3(s)$
$h_{1200} = h_{2100} = 3h_{3000} = 3h_{0300}$	$-h(s)\frac{\sqrt{\beta_x}^3}{8}b_2(s) + \frac{\sqrt{\beta_x}\beta_y}{16}b_3(s)$

with $\delta(s_1), \delta(s_2)$ delta functions at the edge to include the linear effect of a hard edge dipole with edge angle θ needed to obtain a stable unperturbed lattice.

The resonance driving terms can be theoretically derived following the procedure in [8], by writing the perturbation Hamiltonian in complex Courant-Snyder coordinates $h_{q,\pm}$, and identifying $h_{w,jklm}$ as the prefactors of $h^j_{w,x,+}h^k_{w,x,-}h^l_{w,y,+}h^m_{w,y,-}$. The results can be found in Tab. 2.

Application to the HeLICS ring

The first and second order resonance driving terms allow to determine the closed orbit distortion and beta-beating. Compared to a hard edge magnet with edge angles, we find a horizontal closed orbit distortion with a maximum of the order of a millimetre inside the dipoles, and a horizontal (vertical) beta-beating of up to 3% (1%) in the bending units.

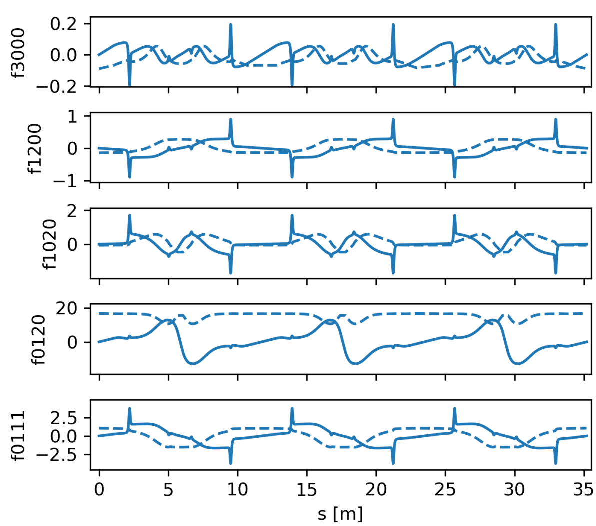

Figure 4: Real (solid line) and imaginary (dashed line) parts of sextupole-like resonance driving terms coming from the dipole fringe field as a function of the position in the ring.

The sextupole-like resonance driving terms can be reconstructed using Eq. (10) as a function of the position in the ring, as shown in Fig. 4. Using the perturbative expansion of the coordinates in Eq. (12) and Eq. (13), one can further reconstruct the spectrum of the ring. This spectrum, taking into account up to sextupole-like spectral lines, is given in Fig. 5 with hard-edge magnet and full magnet decomposition with fringe fields and edge angles. In this figure, one can see less dominant quadrupole-like lines; but broader sextupole-like spectral lines which originate from the decay of the dipole fringe field, the curvature contribution of the quadrupole field and the quadrupole edge angle.

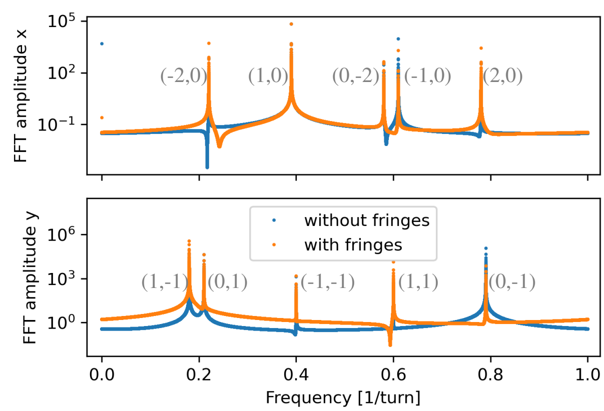

Figure 5: Spectrum of the HeLICS ring with full fringe field effects and edge angles compared to the spectrum for a ring with hard-edge combined function dipoles with only dipole edge angles.

The next steps will be to validate the method with explicit tracking through the field map, and compare the spectral lines to lumped fringe field maps used in several tracking codes. The derivation can be extended to higher-order resonance driving terms and second order perturbation theory, to include effects like the well-known fringe field integral [13] that contributes to additional beta-beating.

CONCLUSIONS

The theory of resonance driving terms can be extended to include the effect of combined-function fringe fields. While additional benchmarking of the predictions is still ongoing, we have shown that this approach allows to determine the contribution to the resonance driving terms everywhere in the ring, which allows taking into account the fringe field and producing field-quality specifications to avoid harmful resonances, or study the impact of a specific design on beam-quality preservation. We have shown that this method can be applied even before a magnet design is available, by creating a magnetic field map based on derivatives on axis.

REFERENCES

[1] H. Huttunen *et al.*, "Optics design of a compact helium synchrotron for advanced cancer therapy", in *Proc. IPAC'24*, Nashville, TN, USA, May 2024, pp. 2991–2994. doi:10.18429/JACoW-IPAC2024-THPC13

[2] E. Benedetto and M. Vretenar, "Innovations in the next generation medical accelerators for therapy with ion beams", in *Proc. IPAC'23*, Venice, Italy, May 2023, pp. 5083–5086. doi:10.18429/JACoW-IPAC2023-THPM090

[3] E. Benedetto *et al.*, "A compact synchrotron for cancer therapy with helium ions", in *Proc. IPAC'25*, Taipei, Taiwan, Jun. 2025, pp. 1159–1162. doi:10.18429/JACoW-IPAC2025-TUPB105

[4] H. Huttunen, F. Asvesta, E. Benedetto, V. Sansipersico, and G. Tranquille, "Orbit error correction schemes for the Helium Light Ion Compact Synchrotron HeLICS", in *Proc. IPAC'25*, Taipei, Taiwan, Jun. 2025, pp. 2236–2239. doi:10.18429/JACoW-IPAC2025-WEPM114

[5] G. Iadarola *et al.*, "Xsuite: An Integrated Beam Physics Simulation Framework", in *Proc. HB'23*, Geneva, Switzerland, Oct. 2023, pp. 73–80. doi:10.18429/JACoW-HB2023-TUA2I1

[6] E. D. Courant and H. S. Snyder, "Theory of the Alternating-Gradient Synchrotron", *Ann. Phys.*, vol 281, no. 1-2, pp. 360-408, Apr 2000. doi:10.1006/aphy.2000.6012

[7] S. Van der Schueren, R. De Maria, E. Benedetto, D. Barna, and M. Migliorati, "Magnetic field modelling and symplectic integration of magnetic fields on curved reference frames for improved synchrotron design: first steps", in *Proc. IPAC'24*, Nashville, TN, USA, May 2024, pp. 1649–1652. doi:10.18429/JACoW-IPAC2024-TUPS09

[8] A. Franchi, L. Farvacque, F. Ewald, G. Le Bec and K. B. Scheidt, "First simultaneous measurements of sextupolar and octupolar resonance driving terms in a circular accelerator from turn-by-turn beam position monitor data", *Phys. Rev. Spec. Top. Accel. Beams*, vol 17, no. 7, Jul. 2014. doi:10.1103/PhysRevSTAB.17.074001

[9] H. A. Enge, *Focusing of Charged Particles*, New York, NY, USA: Academic Press, 1967. doi:10.1016/B978-0-12-636901-4.X5001-9

[10] W. Oelert, "The ELENA Project at CERN", *Acta Phys. Polon. B*, vol. 48, no.10, pp. 1895-1902, 2017. doi:10.5506/APhysPolB.48.1895

[11] S. Van der Schueren, R. De Maria, D. Gamba and M. Migliorati, "Modeling and measurements of the impact of dipole fringe fields in the extra low energy antiproton ring", presented at IPAC'26, Deauville, France, May 2026, paper WEP5085, this conference.

[12] K. Hwang and S. Y. Lee, "Dipole fringe field thin map for compact synchrotrons", *Phys. Rev. Spec. Top. Accel. Beams*, vol 18, no. 12, Dec. 2015. doi:10.1103/PhysRevSTAB.18.122401

[13] E. Forest, S. C. Leemann and F. Schmidt, "Fringe effects in MAD part 1, Second order fringe in MAD-X for the module PTC", KEK, Tsukuba, Japan, Rep. KEK-PREPRINT-2005-109, 2005.